ICAS 2016
30th Congress of the International Council of the Aeronautical Sciences
DCC, Daejeon, Korea ; September 25-30, 2016

EFFICIENT MULTI-RESOLUTION ANALYSIS FOR IMPLICIT TEMPORAL INTEGRATION

Sanghyun Chae*, Hyungmin Kang, Sejong Oh***, Kwanjung Yee***
***Seoul National University, **Dongyang Mirae University, ***Pusan National University**

Keywords: *Multi-Resoultion Analysis, Implicit Temporal Integration, LU-SGS*

Abstract

A novel method has been suggested to improve the computational efficiency of a multi-resolution analysis (MRA) for implicit temporal integrations. The fundamental idea behind MRA is that fluxes are computed only at the points where the gradients of the flow fields are salient, aiming at enhanced computational efficiency. However, the performance of the MRA has a limitation in implicit time integration because the efficiency improvement of the MRA method mostly arises from a reduction in the expensive flux evaluation for spatial discretization. This paper demonstrates that the efficiency of the MRA for implicit temporal integration can be improved by the construction of an additional dataset and a reduced implicit operator matrix. Reducing the implicit operation matrix to fit the size of the dataset decreases the elapsed time of the implicit temporal integration. To limit the numerical error of the implicit operation with the reduced matrix, an additional dataset is constructed by wavelet decomposition with the residuals and a modified thresholding criterion for implicit operation. The accuracy and efficiency of this modified MRA are verified through a complex flow problem of 2D airfoil-vortex interaction. The results show that the computation of the modified MRA with LU-SGS is about 1.7 times faster than that of the original CFD solver, while maintaining the computational accuracy.

1 Introduction

ulti-resolution analysis (MRA) methods have attracted attention as an alternative numerical technique for improving computational efficiency. The main idea of MRA is that on a set of hierarchical grids, the smoothness of flow patterns is determined by the differences between the original values and the approximated values interpolated from the original values discretized on a coarser level grid. In most cases, the differences are sufficiently small in the smooth region. The region where the difference is larger than a certain threshold value can be understood as a region where the gradient of flow property is salient. On the basis of a smoothness evaluation, an adaptive dataset is constructed for the cells in the regions with high gradient of the flow property. High-cost computation such as flux evaluation is performed only in these important regions, and low-cost interpolation is applied in the other regions, resulting in enhanced overall computational efficiency.

The MRA method has been applied to CFD for the enhancement of the calculation efficiency. Harten's pioneering studies[1,2] presented a MRA method for computing discontinuous solutions of hyperbolic PDEs. Holmström[3] proposed an algorithm that used an interpolating wavelet transformation to organize an adaptive data set. Sjögreen[4] also used a MRA method based on an interpolating wavelet transformation to solve the compressible Euler equations. Chiavassa and Donat demonstrated the enhanced computational efficiency in using expensive schemes for shock capturing using a MRA[5,6]. Also, a MRA was applied to grid adaptive strategies of the Finite Volume Method (FVM) for conservation laws and the flow problems by Cohen et al.[7] and Muller and Stiriba[8]. These schemes, which have been called "fully adaptive multiresolution(MR, hereafter)" are cost-efficient. Moreover, significant memory gains can be achieved through the full exploitation of the multilevel structure. Fully adaptive MR,

however, require special data structures in order to obtain the expected memory gains, and its incorporation into an existing code is not straightforward. The cost effective alternative idea proposed in this work, can be incorporated almost as an external routine, at each time step, and implements the easiest scheme to adapt to an existing code.

These MRA concepts turned out to be highly efficient, but previous researchers have not offered reliable error control. To remove this critical weakness, Kang et al.[9, 10] suggested a modified MRA method with the criterion of thresholding. The modified threshold retained the robustness and the accuracy of the conventional solver(CS). Later, Kang et al.[11] extended the MRA method for 3rd order accuracy.

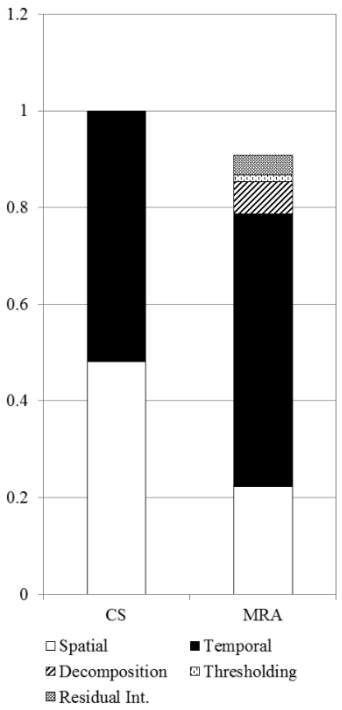

Fig. 1 : Elapsed time comparison of each procedure on implicit temporal integration (LU-SGS).

However, the existing MRA methods have a limitation when applied to implicit time integration methods due to the sparse distribution of the adaptive dataset. Conventionally, all residual values at neighboring cells must be known in advance at one cell for an implicit formulation in a structured grid system. In the adaptive dataset of the MRA, some neighboring cells may be excluded in the adaptive dataset of the MRA, making it difficult for adaptive wavelet implementation on an implicit temporal integration. As shown in Fig. 1, there is a significant reduction in the elapsed time for spatial discretization, but the overall computation remains unchanged due to the portion of the implicit temporal integration. Thus, there is a need to modify the existing MRA for the improvement of the calculation efficiency in implicit temporal integrations.

This paper aims at improving the computational efficiency of the implicit temporal integration while maintain the accuracy of the conventional CFD solver. To this end, construction of an additional dataset and a reduced implicit operator matrix were implemented. The additional adaptive dataset was reconstructed through a wavelet decomposition with the residuals and a modified thresholding criterion for implicit operation. It renders the computational domain split into smooth regions and high gradient regions of the residuals. Then, the implicit operator matrix is reduced to the size of the additional dataset, which consists of the cells in regions of high gradient of the residual. Because the implicit temporal integration should be performed only at the included cells in the adaptive dataset, the reduced implicit operator matrix enhances the computation efficiency on the implicit temporal integration. The usability of the modified method is demonstrated through an aerodynamic analysis of the airfoil vortex interaction. Computational efficiency enhancement is evaluated and compared in a quantitative manner.

2 Numerical Methods

2.1 Baseline Multi-Resolution Analysis on a Euler Solver[11]

In this paper, the two-dimensional Euler equations are used as the governing equations to cover practical transonic problems. The two-dimensional Euler equations are written as Eq. (1).

$$\frac{\partial \boldsymbol{Q}}{\partial t}+\frac{\partial \boldsymbol{E}}{\partial x}+\frac{\partial \boldsymbol{F}}{\partial y}=0 \qquad (1)$$

with $\boldsymbol{Q}=\begin{bmatrix}\rho\\ \rho u\\ \rho v\\ \rho e_t\end{bmatrix}$, $\boldsymbol{E}=\begin{bmatrix}\rho u\\ \rho u^2+P\\ \rho uv\\ (\rho e_t+p)\mathrm{u}\end{bmatrix}$, $\boldsymbol{F}=\begin{bmatrix}\rho v\\ \rho vu\\ \rho v^2+p\\ (\rho e_t+p)v\end{bmatrix}$,

and $e_t=\frac{p}{\rho(\gamma-1)}+\frac{1}{2}(u^2+v^2)$.

To conduct the calculations with an arbitrary curvilinear grid system, these equations are transformed from the Cartesian coordinate system to the generalized coordinate with non-dimensionalization, rewritten as Eq. (2).

$$\frac{\partial \bar{\boldsymbol{Q}}}{\partial \tau}+\frac{\partial \bar{\boldsymbol{E}}}{\partial \xi}+\frac{\partial \bar{\boldsymbol{F}}}{\partial \eta}=0 \qquad (2)$$

with $\bar{\boldsymbol{Q}}=\frac{\boldsymbol{Q}}{J}$, $\bar{\boldsymbol{E}}=\frac{1}{J}\left[\xi_t\boldsymbol{Q}+\xi_x\boldsymbol{E}+\xi_y\boldsymbol{F}\right]$, and $\bar{\boldsymbol{F}}=\frac{1}{J}\left[\eta_t\boldsymbol{Q}+\eta_x\boldsymbol{E}+\eta_y\boldsymbol{F}\right]$.

In this research, the MRA method suggested by Kang et al.[11] was chosen as the baseline. The method is one of latest MRA methods and has advanced features, such as the definition of thresholding value according to the order of spatial accuracy and the convergence acceleration by the restriction. This method uses the interpolating wavelet transformation which includes decomposition and threshold to construct an adaptive dataset on the hierarchical dyadic grid sets, so as to reproduce the local features of the solution. Then, fluxes are calculated only at the points within the adaptive dataset, resulting in improved computational efficiency. The procedures of the CFD solver with the MRA method consist of four steps, as shown in Fig. 2. Step 1. Wavelet Decomposition, Step 2. Flux Evaluation, Step 3. Residual Interpolation, Step 4. Time Integration. A detailed description of each procedure is provided in the Appendix.

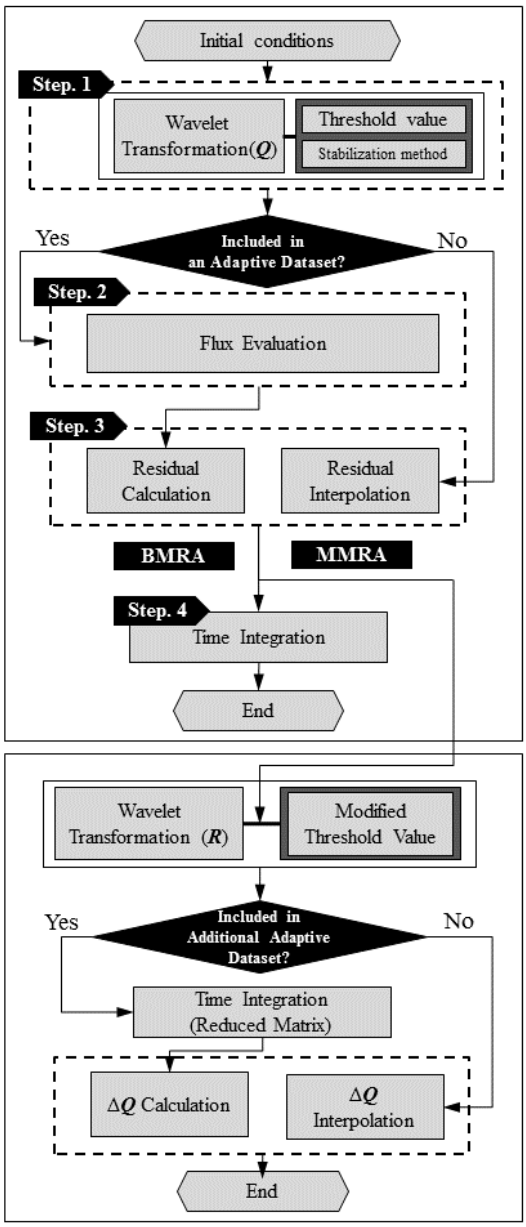

Fig. 2 : Overall procedure of flow simulation with the MRA methods.

2.2 Efficiency Improvement on Implicit Temporal Integration

The simplest way to improve the computational efficiency is to conduct the implicit temporal integration only at cells in the adaptive dataset. If the size of implicit operator matrix is reduced to that of the adaptive dataset, the elapsed time for the implicit calculation will be reduced in the same manner. However, the implicit operation with a reduced matrix can induce numerical error due to the lack of information from neighboring points. To suppress the numerical errors caused by the

reduced matrix operation, an additional adaptive dataset is reconstructed and the new threshold criterion is suggested in the modified MRA (MMRA, hereafter).

Figure 2 shows the flowchart of the MMRA for the efficient implicit temporal integration. The procedures of MMRA are conducted after the residual interpolation of BMRA. Prior to the temporal integration, the additional adaptive dataset is reconstructed. The wavelet decomposition is executed in the same way as the wavelet decomposition of BMRA, shown in Eq. (A1) in the Appendix, except for the substitution of residuals (R) for conservative variables (Q). Then, thresholding is executed with the modified value for the implicit temporal integration. Next, the implicit operator matrix is reduced to fit the size of the additional adaptive dataset to improve the calculation speed of the implicit temporal integration.

To help understanding of the reduced matrix technique, the core idea of the method is best illustrated using an example as in Fig. 3. It is assumed that there are 10 points of 1D structured grid, and six grid points (0, 1, 3, 6, 8, 9) remain in the adaptive dataset after wavelet decomposition and thresholding. In the adaptive dataset, the residual information of excluded cells(2, 4, 5, 7) does not exist; columns of excluded cells are removed and matrix operator is reconstructed as shown in Fig.3 (b) and (c). The reduced size of the implicit matrix shortens the elapsed time for calculating the iterative inversion matrix, which saves significant computational resources.

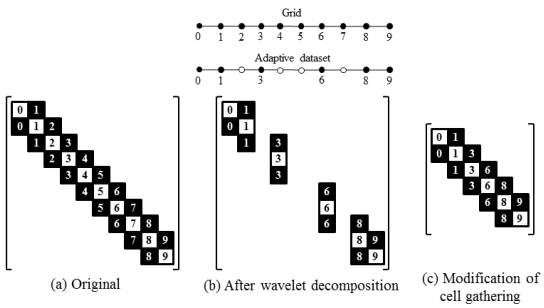

Fig. 3 : Implicit operator matrix for 1-D structured grid.

These modifications of MRA in order to reduce only the size of the matrix, the MMRA can be applied to other types of implicit temporal integration methods. In this paper, temporal integration was conducted with LU-SGS, which is efficient and robust versus alternative direction methods.

3 Results and Discusion

The accuracy and efficiency of the MMRA method are demonstrated on a practical flow problem of a 2-D airfoil vortex interaction. The 2-D transonic airfoil-vortex interaction problem is chosen, because the underlying flow physics are similar to that found in the blade vortex interaction of the helicopter rotor. The capabilities of MMRA are validated under this complex unsteady flow situation, which includes shocks, a moving vortex, and the interactions between the shocks and the vortex. The freestream Mach number is 0.8(Fig. 4). The vortex has a core radius of 0.05c and a nondimensional strength of -0.2. The airfoil has an NACA0012 section. The computation domain is as shown in Fig. 4. (I×J = 336×601 : 217 on the airfoil surface) To preserve the vortex strength, the fine grid region is located in front of the airfoil (gray colored region in Fig. 4).

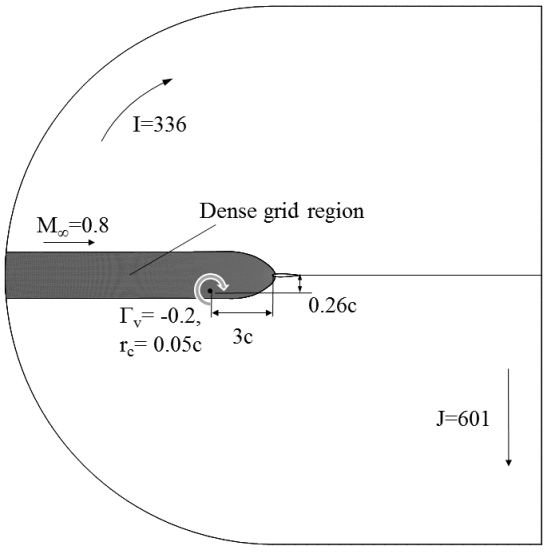

Fig. 4 : Grid system and calculation conditions.

For third-order spatial accuracy, Roe's FDS with Koren's limiter is used and LU-SGS with third-order Euler BDF is used for temporal

integration as in the previous case. Time accuracy is obtained by the reduction of 3 orders of nonlinear residuals by Newton subiteration strategy at each physical time step. The highest level of multi-resolution is level 3 in both MRAs.

Initially, a steady-state solution is obtained for the airfoil-alone configuration, and then the free vortex is released at three chord lengths upstream from the airfoil leading-edge and 0.26 chord lengths below the chord line. Calculations are performed by a marching solution in time with a nondimensional time step size of 0.0005. The released vortex is modeled according to Scully[12]. The clockwise vortex is defined as negative as shown in Fig. 4. The initial pressure and density fields can be established by the radial momentum equation in conjunction with the energy equation for constant enthalpy flows.[13]

Figure 5 shows the variation of lift as a function of the instantaneous streamwise position of the vortex. The lift reaches negative maximum when the vortex travels near the leading-edge and then rapidly increases thereafter. An abrupt change of the moment from positive to negative values is also predicted in Fig 6, as the vortex passes below the airfoil. The variations of lift and moment of CS, BMRA and MMRA method are in reasonably good agreements with those of other Euler and Navier-Stokes investigations[12][14-16].

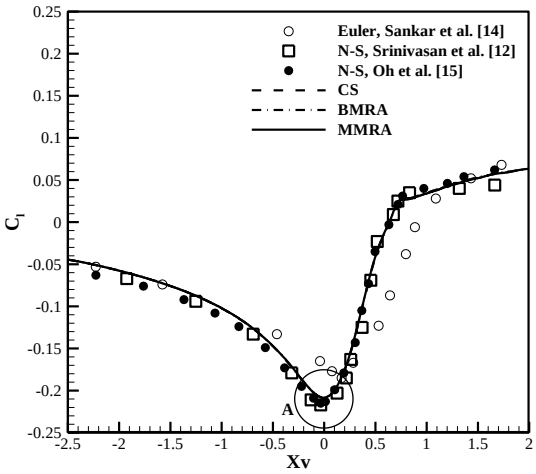

(a) Lift variations in overall region

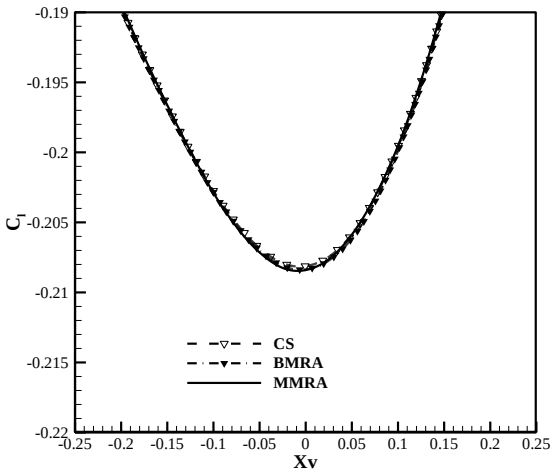

(b) Lift variations at A

Fig. 5 : Comparison of lift variations with the instantaneous vortex position for $M_\infty = 0.8$, $r_c = 0.05c$, $\Gamma = -0.2$ and $y_v = -0.26$.

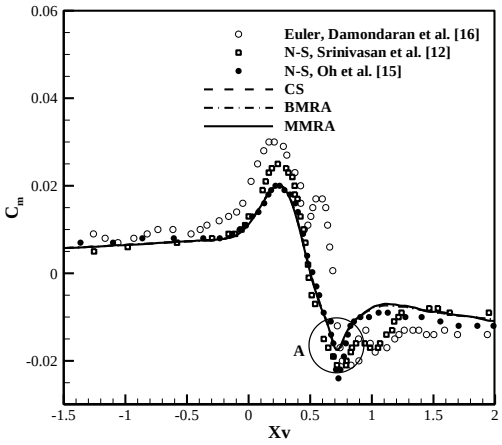

(a) Moment variations in overall region

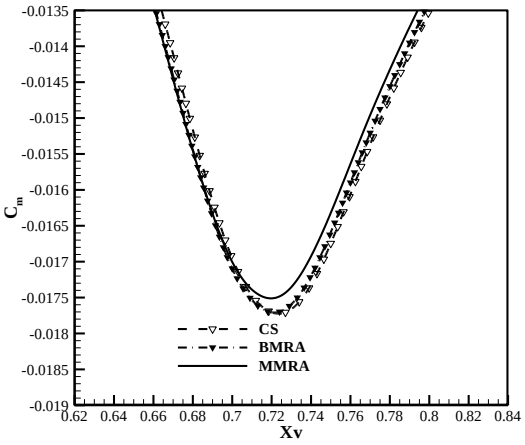

(b) Moment variations at A

Fig. 6 : Comparison of moment variations with the instantaneous vortex position for $M_\infty = 0.8$, $r_c = 0.05c$, $\Gamma = -0.2$ and $y_v = -0.26$

| Pressure contours | Adaptive dataset | Pressure contours | Adaptive dataset |

Xv = -1.5c

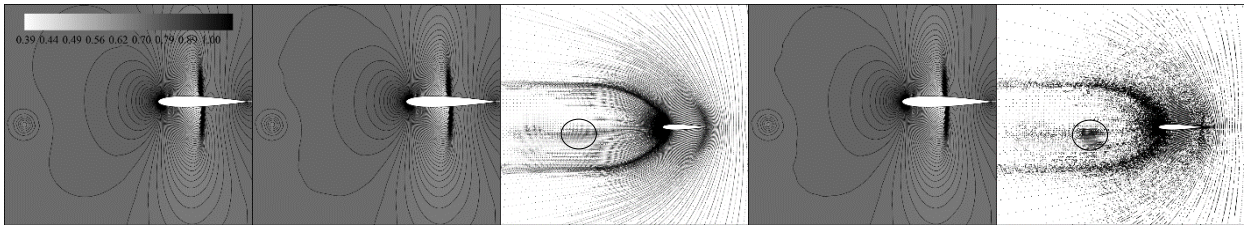

Xv = -1.0c

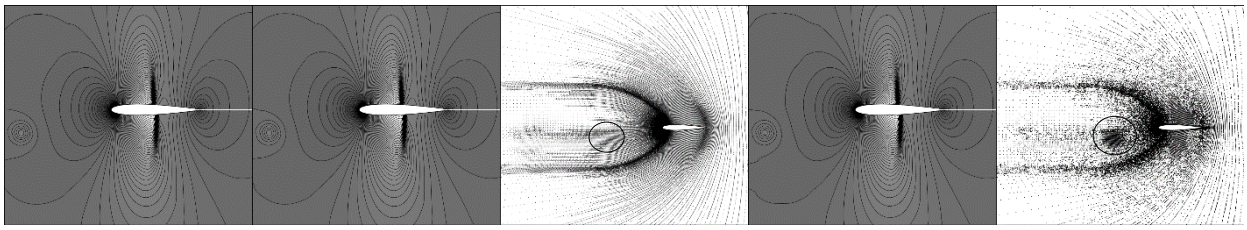

Xv = -0.5c

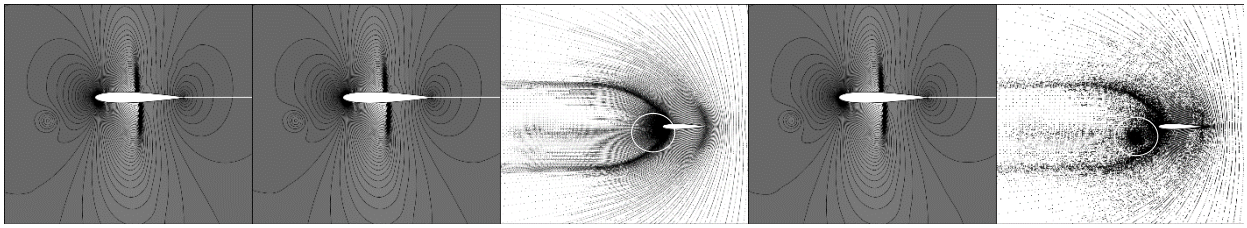

Xv = 0.0c

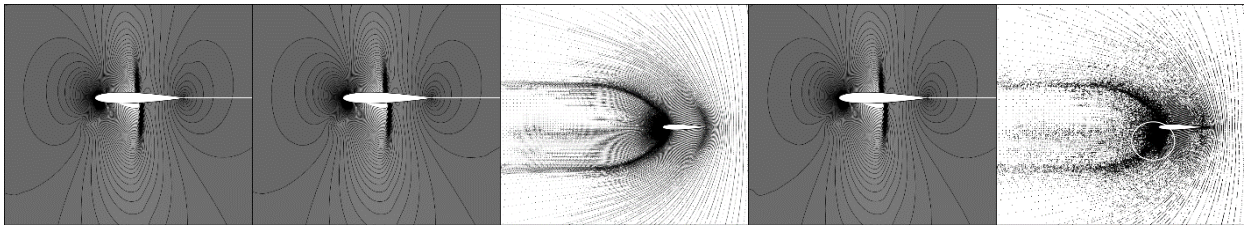

Xv = 0.5c

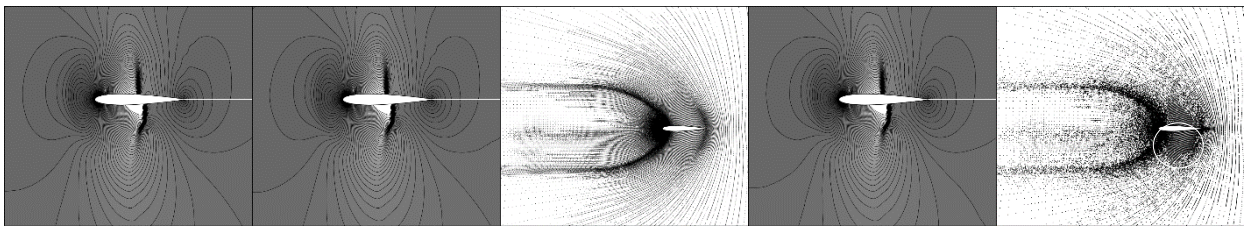

Xv = 1.0c

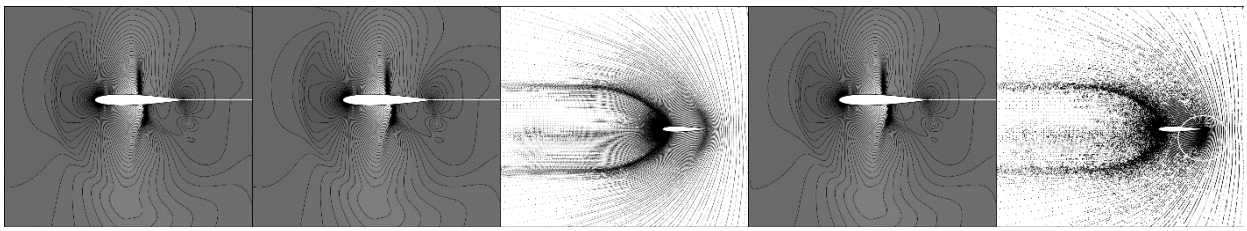

(a) Conventional (b) BMRA (c) MMRA

Fig. 7 : Comparison of pressure distributions and adaptive datasets with the instantaneous vortex position for $M_\infty = 0.8$, $r_c = 0.05c$, $\Gamma = -0.2$ and $y_v = -0.26$.

More details of the analysis of the prediction accuracy follow through comparisons of the pressure distributions. Figure 7 shows the corresponding pressure contours of CS, BMRA and MMRA at six time levels as the vortex passes by the airfoil. Pressure contours clearly illustrate the physical phenomena of the vortex interaction. All test solvers of CS, BMRA and MMRA predict the physical characteristics of the airfoil vortex interaction accurately. Finding differences in the pressure distribution among these solvers is indiscernible to the human eye, because residuals of each cell are decreased below O(10-3) to get temporal accuracy.

The distributions of the adaptive dataset are illustrated in Fig. 7. Comparison between the datasets of BMRA and MMRA indicates that the dataset of MMRA has higher adaptivity than that of BMRA for unsteady simulation. In the dataset of BMRA, the dense grid region around the vortex (in the circle in Fig. 7) cannot be distinguished after Xv = 0c. However, the dataset of MMRA at each time step shows the dense grid region around the vortex (in the circle in Fig. 7). Because the additional dataset of MMRA includes the cells, which have the rapid change of the residuals, i.e. time derivatives, the dataset distribution of MMRA can be more adapted to the instantaneous flow properties in contrast to that of BMRA.

Solver	CPU time (sec.)	Speed-up Ratio	Compression Ratio
CS	5376	1	1
BMRA	4823	1.11	2.05
MMRA	3061	1.76	4.67

Table 1: Results of efficiency improvements in the airfoil-vortex interaction problem.

The calculation efficiency of MMRA is compared with that of BMRA in Table 1. Computation speed of MMRA increased 1.76 times of CS, and 1.59 times of BMRA. The dataset of MMRA is 2.28 times more compressed than that of BMRA. Consequently, it is shown that MMRA improved the computational efficiency and the adaptivity of dataset on the 2-D airfoil vortex interaction problem, while retaining the accuracy of CS. This validation demonstrates that the efficiency enhancement of MMRA is prominent in unsteady simulations in comparison with BMRA.

4 Conclusions

This paper presents MMRA for improved efficiency in the implicit temporal integration. To reduce the elapsed time in the implicit temporal integration, an additional dataset is reconstructed first and the implicit operator matrix is cut down to the size of the additional dataset. In the reduced matrix, diagonal elements of the implicit matrix consist of the cells included in the adaptive dataset and off-diagonal elements are filled with the nearest points to the diagonal cell along the generalized coordinate axis. From the verification and validation of MMRA, the following conclusions are reached:

1) The elapsed time of the implicit temporal integration substantially decreases due to the reduced implicit operator matrix of MMRA. In the airfoil vortex interaction problem, MMRA yielded results 1.6 times faster than CS, while BMRA improved the efficiency only 1.03 times.

2) The dataset of MMRA has the improved adaptivity as proved in the cases of the airfoil vortex interaction. It is because the dataset of MMRA is reconstructed by the wavelet decomposition with the residuals which include the time derivative terms on the unsteady cases.

The suggested strategy can be applied to other types of implicit temporal integration methods because the main idea behind MMRA lies in the reconstruction of the additional dataset and the reduction of the implicit operator matrix. In the final manuscript, numerical robustness and limitations of the suggested method will be demonstrated through the error analysis. Also, the cost reduction by MMRA on aerodynamics analysis of 3-D transonic wing will be presented.

Appendix. Baseline Multi-Resolution Analysis[11]

The wavelet transformation of this method extends the interpolating subdivision scheme presented by Donoho[17]. It is easy to implement with the existing CFD code. The flowchart in Fig.

2 shows the overall implementation of BMRA in the conventional solver. This implementation consists of the following steps.

Step 1. Wavelet Decomposition: To construct the adaptive dataset, decomposition is conducted by interpolating a wavelet transformation. Kang et al. [11] described the decomposition using 6th-order interpolating polynomials for two-dimensional applications.

Assume an initial two-dimensional dyadic grid set in level 1 of the multi-resolution (Fig. A1 (a)). In this figure ◯ cells must be included in the adaptive dataset cells, and are basis points for interpolation. The 6th-order interpolating polynomial evaluates values at other cells, as shown in Eq. (A1). This interpolation is extended at higher levels of the multi-resolution, as shown in Fig. A1 (b).

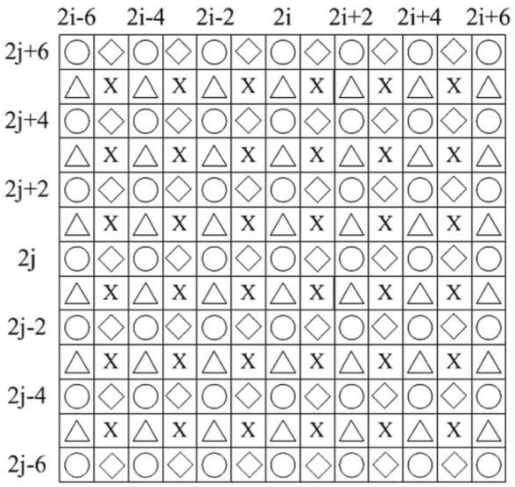

(a) Level k-1

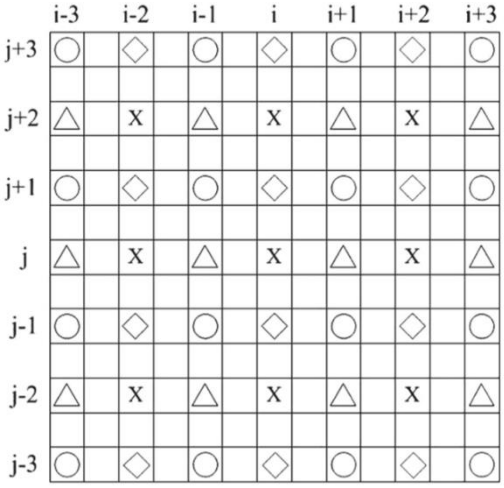

(b) Level k

Fig. A1 : Example of a dyadic grid set on each level[11]

$$\triangle:\ \tilde{Q}^n_{i,j+1}=\frac{1}{256}\left(3Q^n_{i,j-4}-25Q^n_{i,j-2}+150Q^n_{i,j}+150Q^n_{i,j+2}-25Q^n_{i,j+4}+3Q^n_{i,j+6}\right)$$

$$\diamondsuit:\ \tilde{Q}^n_{i+1,j}=\frac{1}{256}\left(3Q^n_{i-4,j}-25Q^n_{i-2,j}+150Q^n_{i,j}+150Q^n_{i+2,j}-25Q^n_{i+4,j}+3Q^n_{i+6,j}\right)$$

$$\times:\ \tilde{Q}^n_{i+1,j+1}=\frac{1}{256}\left(3Q^n_{i-4,j-4}-25Q^n_{i-2,j-2}+150Q^n_{i,j}+150Q^n_{i+2,j+2}-25Q^n_{i+4,j+4}+3Q^n_{i+6,j+6}\right.$$
$$\left.+3Q^n_{i-4,j+6}-25Q^n_{i-2,j+4}+150Q^n_{i,j+2}+150Q^n_{i+2,j}-25Q^n_{i+4,j-2}+3Q^n_{i+6,j-4}\right) \quad \text{(A1)}$$

Then the difference between interpolation value and original value can be derived as Eq. (A2).

$$\triangle:\ d^n_{i+1,j}=\left|Q^n_{i+1,j}-\tilde{Q}^n_{i+1,j}\right|$$

$$\diamondsuit:\ d^n_{i,j+1}=\left|Q^n_{i,j+1}-\tilde{Q}^n_{i,j+1}\right|$$

$$\times:\ d^n_{i+1,j+1}=\left|Q^n_{i+1,j+1}-\tilde{Q}^n_{i+1,j+1}\right| \quad \text{(A2)}$$

If the difference is larger than a thresholding value ε', the point is included in the adaptive dataset as given in Eq. (A3).

$$\varepsilon'=\min\left[\varepsilon,\max\left(\Delta x^l, CFL^m\cdot\Delta x^m\right)\right] \quad \text{(A3)}$$

ε is interpolation error, l means the order of spatial accuracy, m means the order of temporal accuracy. In this study, e is set to $1^{'}\ 10^{-5}$ and third order MUSCL and BDF are used, thus the criterion is applied as Eq. (A4).

$$\varepsilon'=\min\left[10^{-5},\max\left(\Delta x^3, CFL^3\cdot\Delta x^3\right)\right] \quad \text{(A4)}$$

Step 2. Flux Evaluation: After constructing the adaptive dataset, the cells included in the dataset have 1 as the flag value, while the other cells have 0. The flag value of the data set determines whether the flux values are to be evaluated or not. If the flag value is 1, the flux value is calculated by Roe's flux-difference splitting method. Then, MUSCL with a third-order Koren's limiter is applied to evaluate the flux.

Step 3. Residual Interpolation: On the cells in the adaptive dataset, the residual is calculated using the existing CFD code. Residuals on the excluded cells are interpolated in the same way

as that of the interpolating wavelet method, as in Eq. (A5).

$$\triangle:\ \tilde{\boldsymbol{R}}^n_{i,j+1}=\frac{1}{256}\left(3\boldsymbol{R}^n_{i,j-4}-25\boldsymbol{R}^n_{i,j-2}+150\boldsymbol{R}^n_{i,j}+150\boldsymbol{R}^n_{i,j+2}-25\boldsymbol{R}^n_{i,j+4}+3\boldsymbol{R}^n_{i,j+6}\right)$$

$$\diamond:\ \tilde{\boldsymbol{R}}^n_{i+1,j}=\frac{1}{256}\left(3\boldsymbol{R}^n_{i-4,j}-25\boldsymbol{R}^n_{i-2,j}+150\boldsymbol{R}^n_{i,j}+150\boldsymbol{R}^n_{i+2,j}-25\boldsymbol{R}^n_{i+4,j}+3\boldsymbol{R}^n_{i+6,j}\right)$$

$$\times:\ \tilde{\boldsymbol{R}}^n_{i+1,j+1}=\frac{1}{256}\left(3\boldsymbol{R}^n_{i-4,j-4}-25\boldsymbol{R}^n_{i-2,j-2}+150\boldsymbol{R}^n_{i,j}+150\boldsymbol{R}^n_{i+2,j+2}-25\boldsymbol{R}^n_{i+4,j+4}+3\boldsymbol{R}^n_{i+6,j+6}\right.$$
$$\left.+3\boldsymbol{R}^n_{i-4,j+6}-25\boldsymbol{R}^n_{i-2,j+4}+150\boldsymbol{R}^n_{i,j+2}+150\boldsymbol{R}^n_{i+2,j}-25\boldsymbol{R}^n_{i+4,j-2}+3\boldsymbol{R}^n_{i+6,j-4}\right) \quad \text{(A5)}$$

Step 4. Time Integration: For organizing the residual distribution in the whole computational domain, a time integration is performed. Then, the values at the excluded points from an adaptive dataset, i.e. where the flag values are zero, can be neglected if the variations of flow variables, $d\tilde{Q}_{i,j}$ are smaller than the order of the threshold value. This is because the order of variation is within the order of the newly generated errors due to adoption of the adaptive wavelet method. Thus, it is reasonable that we restrict these errors by multiplying an appropriately small value as shown in Eq. (A6).

$$d\tilde{\boldsymbol{Q}}_{i,j}=d\tilde{\boldsymbol{Q}}_{i,j}\times W.F. \quad \text{(A6)}$$

at the exclude points from an adaptive dataset, where

$$W.F=\min\left(\frac{\left|d\tilde{\boldsymbol{Q}}_{i,j}\right|}{\alpha\Delta t\min\left(\frac{0.1}{\Delta x},1\right)\varepsilon'},1\right).$$

The range of α is about $2\le\alpha\le5$ and $\alpha=2$ in this research.

References

[1] Harten, A., "High Resolution Schemes for Hyperbolic Conservation Laws," Journal of Computational Physics, Vol. 49, No. 3, 1983, pp. 357-393.

[2] Harten, A., Enquist, B., Osher, S., and Chakravarthy, S. R., "Uniformly High Order Accurate Essentially Non-Oscillatory Schemes, III," Journal of Computational Physics, Vol. 71, No. 2, 1987, pp. 231-303.

[3] Holmström, M., "Solving Hyperbolic PDEs Using Interpolation Wavelets," SIAM Journal on Scientific Computation, Vol. 21, No. 2, 1999, pp. 405-420.

[4] Sjögreen, B., "Numerical Experiments with the Multiresolution Scheme for the Compressible Euler Equations," Journal of Computational Physics, Vol. 117, No. 2, 1995, pp. 251-261.

[5] Chiavassa, G., and Donat, R., "Point Value Multiscale Algorithms for 2D Compressible Fows," SIAM Journal on Scientific Computation, Vol. 23, No. 3, 2001, pp. 805-823.

[6] Chiavassa, G., and Donat, R., "Shock Vortex Interactions at high Mach numbers," Journal of Scientific Computating, Vol. 19, No. 1-3, 2003, pp. 347-371.

[7] Cohen, A., and Kaber, S. M., Müller, S., and Postel, M., "Fully Adaptive Multiresolution Finite Volume Schemes for Conservation Laws," Mathematics of Computation, Vol. 72, 2003, pp. 183-225.

[8] Müller, S., and Striba, Y., "Fully Adaptive Multiresolution Finite Volume Schemes for Conservation Laws," Mathematics of Computation, Vol. 30, No. 3, 2007, pp. 493-531.

[9] Kang, H., Kim, K., Lee, D., and Lee, D., "Improvement in Computational Efficiency of Euler Equations via a Modified Sparse Point Representation Method," Computer and Fluids, Vol. 37, No. 3, 2008, pp. 265-280.

[10] Kang, H., Kim, K., Lee, D., and Lee, D., "Improved Computational Efficiency of Unsteady Flow Problems via the Modified Wavelet Method," AIAA Journal, Vol. 46, No. 5, 2008, pp. 1191-1230.

[11] Kang, H., Park, K., Kim, K., and Lee, D., "Multi-resolution Analysis for High Accuracy and Efficiency of Euler Computation," International Journal for Numerical Methods in Fluids, Vol. 74, 2014, pp. 661-683.

[12] Srinivasan, G. R., McCroskey, W. J., and Baeder, J. D., "Aerodynamics of Two-Dimensional Blade–Vortex Interaction," AIAA Journal, Vol. 24, No. 10, 1986, pp. 1569-1576.

[13] Srinivasan, G. R., and McCroskey, W. J., "Numerical Simulations of Unsteady Airfoil-Vortex Interactions," Vertica, Vol. 11, No. 1, 1987, pp.3–28.

[14] Sankar, N. U. and Malone, J. B., "Unsteady Transonic Full Potential Solutions for Airfoils Encountering Vortices and Gusts," AIAA Paper 85-1710, 1985.

[15] Oh, W. S., Kim, J. S. and Kwon, O. J., "Numerical Simulation of Two-Dimensional Blade-Vortex Interactions Using Unstructured Adaptive Meshes," AIAA Journal, Vol. 40, No. 3, 2002, pp.474–480.

[16] Damodaran, M., and Caughey, D. A., "Finite Volume Calculation of Inviscid Transonic Airfoil–Vortex Interaction," AIAA Journal, Vol.26, No.11, 1988, pp. 1346–1353.

[17] Donoho, D. L., "Interpolating wavelet transforms," Technical Report 408: Department of Statistics, Stanford University, 1992.

5 Contact Author Email Address

Kwanjung Yee, kjyee@snu.ac.kr

Copyright Statement